Identification of spatial pattern of photosynthesis hotspots in biological soil crusts by combining chlorophyll fluorescence imaging and multispectral NDVI images

Andreas Kleefeld[a], Stella Gypser[b*], Werner B. Herppich[c], Georg Bader[d], Maik Veste[b,e]

[a]Forschungszentrum Jülich, Institute for Advanced Simulation, Jülich Supercomputing Centre, Wilhelm-Johnen-Straße, 52425 Jülich, Germany

[b]Brandenburg University of Technology Cottbus-Senftenberg, Soil Conservation and Recultivation, Konrad-Wachsmann-Allee 6, 03046 Cottbus, Germany

[c]Leibniz-Institute for Agricultural Engineering and Bioeconomy, Department Horticultural Engineering, Max-Eyth-Allee 100, 14469 Potsdam, Germany

[d]Brandenburg University of Technology Cottbus-Senftenberg, Numerical Mathematics and Scientific Computing, Platz der Deutschen Einheit 1, 03046 Cottbus, Germany

[e]University of Hohenheim, Department of Botany, Garbenstraße 30, 70599 Stuttgart, Germany

*corresponding author: stella.gypser@b-tu.de

Abstract

Although biological soil crusts can be found in open landscapes worldwide, their species composition strongly depends on microclimate and their respective developmental stage. In addition, local variations in water holding capacity and/or chemical properties of soils influence the formation of spatial patterns and different types of biocrusts on the landscape level. For the evaluation of biocrusts functions and their impact on soil carbon pools, the analysis of the

interrelationship between photosynthetic activity and the variations of spatial distribution pattern and types of biocrust is indispensable. For this purpose, an image processing approach was applied that combined chlorophyll fluorescence analyses and multispectral NDVI to comprehensively characterize the spatial patterns of photosynthetic hotspots in biological soil crusts. For image analysis, five biological soil crust types with different ratios of bare substrate, mosses and lichens were collected on an inland dune system in Lieberose, dominated by the moss *Polytrichum piliferum*, and the lichens *Cladonia fimbriata* and *C. coccifera*. RGB-images of the biocrusts were taken with a standard consumer camera Nikon 5200, NDVI images with a modified Canon S110 NIR camera and chlorophyll fluorescence images with a modular open FluorCAM FC 800-O/1010, respectively. NDVI and F_v/F_m were nearly in the same range for all biocrust samples, although mosses always showed higher NDVI than lichens. F_0 and F_m increased with species coverage and with advancing biocrust development. Overlapping of NDVI with F_0 and F_m images showed that not all crustal organisms contribute to NDVI and chlorophyll fluorescence. The overlapping areas of NDVI and F_0 ranged between 13 % and 29 %, that of NDVI and F_m between 17 % and 47 %. Generally, matching of RGB, NDVI and chlorophyll fluorescence images showed that photosynthetic performance of mosses was higher than that of lichens and, hence, these species represented the hotspots of photosynthesis in biocrusts.

Keywords: biocrusts, image analysis, NDVI, chlorophyll fluorescence, spatial pattern

1. Introduction

In many ecosystems, the soil surface is settled by various species of cyanobacteria, bacteria, green algae, mosses, liverworts, lichens and fungi (Belnap and Lange, 2003). In addition, biological soil crusts (biocrusts) can be found in various open landscapes with sparse vegetation worldwide, e.g. in polar regions, coastal and inland sand dunes, grasslands and initial ecosystems (Cutler et al., 2008; Schaaf et al., 2011; Pushkareva and Elster, 2013). Comprehensive studies on structure and function of biocrusts, however, were nearly exclusively conducted in arid and semi-arid areas (Johansen, 1993; Breckle et al., 2008; Maestre et al., 2011; Weber et al., 2016). Characteristic for biocrusts is their three-dimensional structure, which initially has been formed by microorganisms cross-linking soil particles and developing a top layer on the soil surface. The thickness of the crusts can vary from a few millimeters to several centimeters. The species composition depends on microclimatic conditions and the development stage of biocrusts (Büdel and Veste, 2008; Gypser et al., 2015). For early stages, green-algae and cyanobacteria are particularly characteristic. In contrast, mosses dominate the cryptogamic communities in mid-succession, while soil lichens occur only in late successional stages (Eldrige and Greene, 1994; Gypser et al., 2015).

Even if biocrusts are covering only the topsoil, they are key drivers for functional processes and the development of ecosystems (Schaaf et al., 2011; Veste al., 2001). Due to their specific features, biocrusts can serve as model systems in ecosystem theory and their analysis may help to understand the interactive processes occurring during soil formation and ecosystem development (Bowker et al., 2010; Schaaf et al., 2011; Maestre et al., 2016). Biocrusts stabilize the soil surface (Breckle et al., 2008), influence the soil hydrological processes (Kidron et al., 1999; Li et al., 2016), and accumulate organic carbon (Dümig et al., 2014) and macro- and micronutrients

(Russow et al., 2005; Brankatschk et al., 2013; Yu et al., 2016).

As rootless poikilohydric organisms, the photosynthetic activity of biocrusts strongly depends on moisture supply from dewfall, fog and/or rainfall. Differences in microclimatic conditions and water holding capacity of biocrusts, and, at least partly, in chemical properties of soils can explain the formation of spatial patterns of different biocrust types. Especially the duration of soil surface wetness is most important for the physiological activity of biocrusts, and for the formation of different types of biocrusts on the landscape level (Veste and Littmann, 2006; Veste et al., 2008).

Therefore, the evaluation of photosynthesis in relation to the variation in spatial distribution patterns of the biocrusts is very important for understanding their functions. The photosynthetic activity of biocrusts can easily be monitored by chlorophyll fluorescence analyses (CFA; Schroeter et al., 1991, 1992; Veste et al., 2001; Raggio et al., 2014). Common chlorophyll fluorescence devices use fiber optics (approximately 6 mm diameter) and, thus, provide only very local information of physiological activity of biocrusts but not on its spatial variations. In contrast, current chlorophyll fluorescence imaging systems may resolve this limitation (Bauriegel and Herppich, 2014). In fact, this technique has yet been successfully applied to various biocrust types (Pushkareva et al., 2013; Gypser et al., 2016).

On the other hand, Normalized Difference Vegetation Index (NDVI) imaging may help analyzing the spatial heterogeneity and distribution of chlorophyll (Bauriegel et al., 2011a). Consequently, this parameter was successfully applied to investigate biocrusts at different spatial scales (Burgheimer et al., 1993; Karnieli and Tsoar, 1995). Recently, modified low-cost consumer cameras proved an interesting and simple alternative for the complex multispectral monitoring of NDVI in the field and in the laboratory. These cameras also can easily be mounted on different

micro-drones to record NDVI on the field scale (Läderach et al., 2015). These high resolution NDVI-camera systems are also suitable for the ground-based evaluation of distribution patterns of biocrusts (Fischer et al., 2012; Gypser et al., 2016). In addition, they allow novel applications for small-scale monitoring of biocrusts.

The combination of both CFA and NDVI may actually allow further comprehensive analyses of the spatial variations of photosynthetic activity (Bauriegel et al., 2011b) but are still lacking for biocrusts. These analyses are, however, essential to better understand the mechanisms of biocrust formation and the influence of various environmental factors (e.g. microclimate, drying, shading or surface properties of soils) on the development of various types of crusts. It was shown that photosynthesis is not uniformly distributed on the biocrust surface or over the specific crustal community (Gypser et al., 2016; Schroeter et al., 1992). The characterization and quantification of these spatial patterns is, however, still an open issue. Hence, by combination of CFA and NDVI imaging, the presented study aims to identify the hotspots of photosynthesis and their spatial pattern in biocrusts. These hotspots are related to the specific metabolic competence characterizing the particular species determining the differing spatial distribution patterns, which, in turn, provide essential information on the respective developmental stage of biocrust. For this purpose, CFA and NDVI images of field-sampled biocrusts, differing in their species composition were taken by different camera systems. An image processing approach was developed to combine CFA and NDVI images and facilitate the identification of hotspots of photosynthesis.

2. Materials and methods

2.1. Biological soil crusts

Samples of biological soil crusts were collected in an inland dune system (51°55'35" N, 14°20'05" E) near Lieberose (Lower Lusatia, Brandenburg, Germany). The Lower Lusatia region is characterized by the transitional Atlantic to continental climate with a mean annual temperature of 9.3°C and a mean annual precipitation of 581 mm a^{-1} (1981 to 2010) recorded at the nearest climate station in Cottbus (DWD, 2014). In 2016, a mean annual temperature of 9.5°C and a total annual precipitation of 632 mm a^{-1} were recorded (DWD, 2017).

The crusts were taken from an inland dune with dry acidic grassland dominated by *Corynephorus canescens* and heath dominated by *Calluna vulgaris* (Ellenberg and Leuschner, 2010). For image analyses, five biocrust types (BC 1 to BC 5) with different ratios of moss, soil lichens and bare substrate cover were collected to enable image analyses with varying distribution patterns. Samples BC 1 and BC 2 were dominated by the moss *Polytrichum piliferum*. While BC 1 showed high moss coverage of nearly 90 %, BC 2 contained mosses just on a half of the overall area resulting in an estimated surface coverage of 60 %. The biocrust samples BC 3 and BC 4 contained a mixture of the moss *Polytrichum piliferum* and soil lichens of the genus *Cladonia*. Both biocrust samples had a surface coverage of almost 95 %, while the mosses and lichens contribute in equal parts. Whereas lichens occurred just on one half of the surface area of BC 3, they covered the whole area in BC 4. The surface area of BC 5 was totally covered, dominated by the soil lichens *Cladonia fimbriata* and *C. coccifera*, but the crust also contained mosses of the species *Polytrichum piliferum*. The samples were collected by gently coring Petri dishes (10 cm × 10 cm) in the upper soil layer. Ruptures were carefully avoided to obtaining well-defined surface areas easily comparable between samples. The fact that Petri dishes were quadratic and the added

marking labels facilitated matching of the respective RGB, NDVI (red labels) and chlorophyll fluorescence (blue labels) images.

2.2. RGB-images

RGB images of the five biocrust samples were recorded with a standard consumer camera Nikon 5200 (Nikon, Tokyo, Japan) equipped with a standard 35 mm objective and a resolution of 6000 pixels × 4000 pixels.

2.3. NDVI images

NIR-Green-Blue (NIR-G-B) images were taken with a modified Canon S110 NIR camera (Drones Imaging, Maisons Laffitte, France) with a resolution of 4000 pixels × 3000 pixels (for details see Läderach et al., 2015). The NIR-G-B camera excludes visible light in the red spectral range (630 nm to 700 nm), while the blue (450 nm to 490 nm), the green (490 nm to 560 nm), and the near infrared band (700 nm to 1300 nm) were recorded. Chlorophylls absorb in the blue and the red but not in the green or in the near infrared spectral range (Bresinsky et al., 2008). Thus, NDVI images for each biocrust samples was calculated by the offsetting of the blue (B) and the near infrared (NIR) channel as

$$NDVI = \frac{NIR - B}{NIR + B} \in [-1,1]$$

The NDVI images were converted to a gray valued image in two steps. First, each tonal value was shifted to the interval [0,2] and, secondly, these values were adapted to the NDVI scale ranging from 0 to 1. The respective NDVI values were calculated by using the median of the tonal values in the range from 0 to 255 for each biocrust NDVI image, scaled in the interval [0,1]. Therefore, the NDVI was calculated as (Fischer et al., 2012; Gypser et al., 2016):

$$NDVI = \frac{Median\ tonal\ value}{255}$$

2.4. Chlorophyll fluorescence imaging

Chlorophyll fluorescence imaging (CFI) was performed with an open modular system (FluorCAM FC 800-O/1010, PSI, Brno, Czech Republic) measuring sequences of fluorescence images with a user-defined timing of set points, measurement intervals, and irradiance. The recommended size of the experimental objects was 10 cm × 10 cm, which included the entire biocrust sample. Fluorescence was induced by two sets of super-bright orange LEDs (λmax = 620 nm) that provide light pulses of variable duration (10–33 μs) and photon fluence rates. Short-term (1 s) closure of photosystem II was induced by saturation light pulses (> 2500 μmol photons m^{-2} s^{-1}) generated by two panels of super-bright white LEDs. Before measurements, samples were carefully moistened, pre-darkened for 15 min and then illuminated with weak red light (approximately 3 μmol m^{-2} s^{-1}) for 3 s to induce the initial fluorescence (F_0). Then the maximum fluorescence signal (F_m) was elicited by the saturation pulse. The ratio F_v /F_m (F_v = F_m − F_0 = variable fluorescence) is an indicator of the potential maximum photochemical efficiency and can be used to determine both capacity and stability of photosynthesis, and its response to external constraints (von Willert et al., 1995).

A CCD camera, fitted with an F1.2/2.8-6 mm objective and a short pass filter, recorded gray valued fluorescence images (512 pixels × 512 pixels resolution). The chlorophyll fluorescence signals of each image were decoded as gray values (range 0 and 1000; 0=black and 1000=white) to facilitate the extraction of relevant information such as the location of hotspots i.e. the regions of high chlorophyll fluorescence emission. For visual comparison of chlorophyll fluorescence images, they were scaled according to the minima and maxima of all biocrusts in the range from 0 to 1600 (relative units) for F_0 and F_m, and from 0 to 0.9 (relative units) for F_v/F_m. The weighted

mean of F_0, F_m and F_v/F_m were calculated for all biocrust samples.

2.5 Matching of NDVI and chlorophyll fluorescence images

The gray valued chlorophyll fluorescence images consisted of pixels with tonal values in the range from 0 to 255, where 0 was assessed as black and 255 as white, and hence, belonged to low or high chlorophyll fluorescence, respectively. Prior to the matching of NDVI and chlorophyll fluorescence images, the separate chlorophyll fluorescence images of F_m and F_0 were divided into three classes. The first class included pixels with tonal values ranging from 0 to 25, which were excluded from the image matching, because this tonal range reflected particularly the substrate without chlorophyll fluorescence and could lead to a false response of these tonal values. The second class consisted of pixels with tonal values in the range from 25 to 35 for F_0 and 25 to 60 for F_m and represented areas with low chlorophyll fluorescence. The different threshold determination of CFI for F_0 and F_m was carried out by applying an empirical cumulative distribution function (CDF):

$$F_n(t) = \frac{1}{n}\sum_{i=1}^{n} 1_{x_i \leq t}$$

where $F_n(t)$ describes the empirical distribution function, n is the sample size, $1_{xi \leq t}$ is a Bernoulli random variable for a fixed t (tonal value) with parameter $p = F(t)$, and 1_A denotes the indicator function of an event A. An 80 % quantile of the five biocrust images were set to differentiate between areas with low or high chlorophyll fluorescence (Fig. 1). These empirical CDF values amounted 0.76, 0.86, 0.81, 0.81 and 0.82 for F_0, and 0.88, 0.86, 0.74, 0.75 and 0.85 for F_m of the samples BC 1 to BC 5, respectively, which resulted in gray tonal values of 35 for F_0 and 60 for F_m. The above mentioned thresholds of 25, 35 and 60 were related to normalized chlorophyll fluorescence values of 156.9, 219.6 and 376.5, respectively.

For the detection of hotspots of photosynthesis within different biocrust samples, clippings of the NDVI and the chlorophyll fluorescence images were matched to the RGB images. Therefore, the visible markers on RGB, NDVI and CFA images were used. Both F_0 and F_m images were used for matching, since the F_m signals visualize the spatial distribution of the metabolic active chlorophylls, while F_0 reacted more sensitive to desiccation of biocrusts (Veste et al., 2001). On the basis of these matches, both the biocrust species with high chlorophyll content and those with high photosynthetic activity could be identified. Following, the area ratio of NDVI or chlorophyll fluorescence-related area and the ratio of the overlapping areas of NDVI, F_0 and F_m were determined. The visible markers on the biocrust images used for matching were removed manually from the pictures before data processing to avoid a mistakenly inclusion during the calculation of the spatial chlorophyll fluorescence.

3. Results

3.1 Structure of biocrust samples

In the RGB images, the moss *Polytrichum piliferum* dominated BC 1 but with several spots of the bare soil substrate (Fig. 2). The sample BC 2 showed similar patterns with an intensive contribution of mosses only on one half of the biocrust but a sparse one on the other. In BC 3, fruticose soil lichens of the genus *Cladonia* appeared in addition to the mosses. While two-thirds of the whole biocrust was covered with this moss-lichen community, one-third was purely covered with mosses. Furthermore, BC 4 showed a distinctive moss-lichen community on the entire biocrust, while BC 5 was characterized by a spatial mixture of mosses in between larger *Cladonia* thalli. For the comparison of the effect of spatial crust pattern on NDVI and CFI, the moss-dominated biocrust BC 1, the lichen-dominated biocrust BC 5, and BC 4 as a transient

stage between moss- and lichen- biocrust were selected.

3.2 Normalized Difference Vegetation Index

The RGB images as well as the corresponding NIR-G-B and gray valued NDVI images of all biocrust samples are summarized in Fig. 2. The comparison of the three image types highlights the advantage of the NDVI over the RGB images for the evaluation of the distribution of various biocrust components. NDVI also facilitates the differentiation of components according to their relative physiological activity. Nevertheless, the NDVI of all biocrust images ranged between 0.59 and 0.68 (Tab. 1). The minor difference between the NDVI of BC 1 (0.65) and that of BC 2 (0.59) can be explained by the lower coverage with mosses in BC 2.

3.3 Chlorophyll fluorescence

Means of F_0 and F_m obtained for images of the samples BC 1 and BC 2 were approximately 20 % lower than those calculated for images of BC 3 to BC 5 (Tab. 1). For the latter biocrust samples nearly the same means of F_0 and F_m were recorded. For all biocrust samples, the ratio of F_v/F_m is lowest in BC 1 and highest in BC 2; while BC 3 to BC 5 showed a similar F_v/F_m ratio. Overall, NDVI and F_v/F_m were in the similar range for all biocrust samples. Consequently, correlation analysis of NDVI and chlorophyll fluorescence parameters clearly yielded the same clustering of the biocrust samples (not presented here). The respective images of all three chlorophyll fluorescence parameters analyzed showed nearly the same variation in the spatial distribution of the biocrusts as those of NDVI (Fig. 3).

3.4 Matching of NDVI and CFI

Automatic matching of entire biocrust images obtained with the two cameras, which differ in both position and resolution, did not work satisfyingly. Consequently, matching of a smaller portion of the images was done manually (e.g. Fig. 4). For comparison of matching results of

NDVI, F_0 and F_m images, the biocrust samples BC 1 and BC 5 were chosen due to their pronouncedly differing composition regarding mosses and lichens. BC 4 was included as a biocrust type, which contained both mosses and lichens and represented a transition from BC 1 to BC 5. Pre-determined thresholds of 35 and 60, respectively, were applied to create the red-colored areas of F_0 and F_m, while the NDVI was blue-colored in the clipped images (Fig. 4 to 6, Appendix Fig. A1 and A2 of BC 2 and BC 3).

The calculated area ratio of NDVI pixels relative to the total area of the clipped RGB-images ranged between 47.7 % and 84.0 % for all biocrust samples (Tab. 2). The area ratio of F_0 for the matching of low chlorophyll fluorescence values (8.1 % to 16.4 %) was slightly higher with a mean of 13.7 ± 3.4 % compared to the area ratio for the matching of high chlorophyll fluorescence values (9.9 % to 13.6 %) with a mean of 11.6 ± 1.5 %, respectively. The area ratio of F_m for the matching of low chlorophyll fluorescence values (21.5 % to 37.6 %), however, was clearly higher with a mean of 27.4 ± 6.6 % compared to the area ratio for the matching of high chlorophyll fluorescence values (10.2 % to 24.0 %) with a mean of 16.5 ± 5.5 %, respectively. The spatial ratios of F_0 or F_m did not necessarily coincide with those of NDVI, irrespective of the biocrust (Fig. 4 to 6 (D)).

The overlapping areas of NDVI and F_0 (Fig. 4 to 6 (E)) ranged between 16.3 % and 25.4 % for the low chlorophyll fluorescence values, and between 13.2 % and 28.5 % for the high chlorophyll fluorescence values, respectively (Tab. 2). For the matching of NDVI and F_m, the overlapping areas ranged between 32.4 % and 47.1 % for the low chlorophyll fluorescence values, and between 17.0 % and 37.3 % for the high chlorophyll fluorescence values, respectively. Hence, the overlapping areas were higher for the NDVI/F_0- and NDVI/F_m-matching in the low chlorophyll fluorescence value range compared to the high chlorophyll fluorescence value range. Also, the

spatial area matching of NDVI/F_m was higher compared to the corresponding matching of NDVI/F_0.

4. Discussion

4.1 Influence of biocrust composition on NDVI and CFA images

In spite of similar NDVI values of BC 1 and BC 5, the imaging of NDVI (Fig. 2) and the overlapping areas of NDVI and chlorophyll fluorescence (Fig. 4 and 5 (D)) clearly showed a higher NDVI of mosses compared to lichens. This effect may result from the layered structure of lichens. The photosynthetic active symbiont (photobiont) is located inside of the vegetation body, which is basically formed by fungal mycelia. This covering layer, in turn, may reduce light absorption by chlorophylls. In addition, the total chlorophyll content can be lower in single lichens. Clear differences in the spectral reflectance between moss biocrusts and soil lichens were also reported by Weber et al. (2008) and Rodriguez-Caballero et al. (2015). The NDVI of moss dominated biocrusts with high coverage was higher than that found for moss-lichen dominated biocrusts. Even a higher amount of fully-developed lichens could not significantly affect the mean NDVI.

The analysis of NDVI, F_0 and F_m indicate a specific response of parts of the mosses and lichens, i.e. not all crustal organisms contribute to both NDVI and CFA. Especially the overlapping of NDVI images with those of F_0 and F_m showed that not the entire biocrust community, which contain chlorophyll and showed a response in the NDVI imaging, were also photosynthetic active in both the low or high chlorophyll fluorescence range (e.g. Fig. 5 and 6). Although some distinct lichens showed photosynthetic activity in the high F_m range (Fig. 5), photosynthetic performance of mosses was continuously higher. Hotspots of photosynthesis were characterized by both high

NDVI and chlorophyll fluorescence, reflecting a high photosynthetic activity and, hence, mosses formed the hotspots of photosynthesis of the whole biocrust.

Reportedly, mosses may absorb higher amounts of water than lichens (Gypser et al., 2015b; Veste et al., 2011; Yair et al., 2011). The spatial imaging of F_v/F_m indicated that the maximum photochemical efficiency of the biocrusts was always located beneath the biocrust surface (Garcia-Pichel and Belnap, 1996; Raanan et al., 2015). The marginal areas of biocrust were only poorly visible in the respective parts of both F_m and, more pronounced, of F_v/F_m images. It may be assumed that biocrust at the edge desiccated faster. On the other hand, more liquid water may have been concentrated in the middle of the samples although care was taken to equally moisten all biocrusts prior to chlorophyll fluorescence measurements. Despite the fact that means of F_v/F_m were in the same range for all biocrusts, a clear variation in spatial distribution patterns of photosynthetic capacity among the different biocrust samples is obvious in the multispectral and fluorescence images.

Both F_0 and F_m allow the analysis of specific photosynthetic responses to various environmental constraints (von Willert et al., 1995); consequently both parameters were included in the matching process. It was observed that during desiccation, F_0 reacted more sensitively than F_m (Veste et al., 2001). Therefore, it affected the effective quantum yield F_v/F_m (Veste et al., 2001) and may be advantageous in investigations of the moisture-dependent physiological active phase. On the other hand, F_m was shown to be preferable for the evaluation of the spatial distribution of photosynthetic activity of biocrusts (Gypser et al., 2016).

The correlation of NDVI withF_0, F_m and F_v/F_m may point to a clustering of the sampled biocrusts as previously reported by Gypser et al. (2016). These authors showed that some relation of these parameters may be due to the changes of species compositions during biocrust development. For

fully developed biocrusts, composed of both mosses and lichens, highest values of F_0 and F_m corresponded with highest NDVI (Tab. 1). The evaluated biocrust samples, however, were not selected to analyze the physiological changes during biocrust development but should optimally reflect the successional stage of fully developed biocrusts (Gypser et al., 2016). In general, the ecophysiological performance of biocrusts can be related to their specific community composition. There could be a sigmoidal light saturation behavior of photosynthetic performance in fully developed biocrusts. Also, the spatial ratios with high or low chlorophyll fluorescence and hence, photosynthetic activity depends on the community composition and surface coverage of biocrusts. Indeed, F_0, F_m and F_v vary with the specific biocrust composition. Areas with high photosynthetic activity, i.e. the photosynthetic hotspots, however, represent only a smaller portion compared to those with low photosynthetic activity. Related to the chlorophyll containing biocrust parts, visible in NDVI images, the hotspots including high F_0 and F_m amounted 42.2 ± 10.9 %, while the areas with lower photosynthetic activity amounted 60.0 ± 5.1 % of the total sample surface area. Spatial photosynthetic activity should be considered in the evaluation of the influence of different biocrust types in the analysis of carbon cycles and carbon accumulation in initial soils, and finally, improvement of soil quality and functions (Dümig et al., 2014).

4.2 Methodical consideration

Matching of images obtained with two cameras, which generally differ in both position and resolution, was challenging. Assuming that the planes of both biocrust samples and cameras were parallel, the images were transformed to a joint coordinate system by using displacements, scaling, and plane rotations. If the two planes were not perfectly parallel, the images were distorted three-dimensionally. This could not be easily corrected due to the lack of relevant information. In particular with inexpensive consumer cameras, the optical angle becomes larger

with large objects. This causes additional optical errors uncorrectable without specific knowledge of camera systems and optics. Finally, some alterations of samples structure due to handling (transportation, watering, etc.) might have occurred between the acquisitions of the different images. For the above reasons and the fact that the images were quite different in content, automatic image registration algorithms might have been not able to closely match the pictures adequately. Hence, manually matching of small parts of the images was preferred.

The use of thresholds for determining regions of low or high chlorophyll fluorescence enabled the differentiation between biocrust species and their contribution on the total photosynthetic capacity. The thresholds determined for the gray valued images seemed to be a reliable parameter, which can be used for comparable image analysis. If the selected threshold were too high, the areas representing high chlorophyll fluorescence signals were smaller and vice versa. This can lead to some uncertainties, complicating the direct comparison between different biocrust types. A next step for a more detailed spatial pattern analysis should be the inclusion of whole biocrust images and CFI with their original chlorophyll fluorescence scale.

Rasmussen et al. (2016) used consumer-grade cameras on unmanned aerial vehicles to obtain vegetation indices from remote images of cereal crops. These authors observed that the angular variations of reflectance showed varying brightness according to the incident sun radiation. This bidirectional reflectance led to deceptive conclusions under sunny conditions. But they also proved the usability of consumer-grade cameras as simple and inexpensive alternatives to expensive multi-spectral sensor systems for the spatial analysis of NDVI.

Compared to former studies using the camera type Olympus Camedia 5000z with a separate Hoya R72 infrared filter (Fischer et al., 2012; Gypser et al., 2016), the novel application of the NIR-G-B camera allowed a faster and easier imaging, because no separate NIR-filter needs to be

mounted on the camera. As a consequence, post-proceeding steps such as positioning the separate RGB, VIS and NIR images to each other for further image processing can be omitted. Furthermore, the higher resolution of 4000 pixel × 3000 pixel (Canon) compared to 1024 pixel × 768 pixel (Olympus) reduced the concomitant inaccuracies and allowed more detailed analyses of NDVI images.

4. Conclusions

NDVI and F_v/F_m were nearly in a similar range for all biocrust types, independent of their spatial pattern distribution. However, NDVI imaging revealed a higher chlorophyll content of mosses compared to lichens.

In addition, matching of NDVI images with CFI indicated a higher photosynthetic performance of mosses. F_0 and F_m increased with species coverage and advancing biocrust development. Hence, mosses represented hotspots of photosynthesis of the whole biocrust and the ecophysiological performance of biocrusts can be related to their species composition. However, these hotspots of photosynthesis represent only a smaller part of the biocrust compared to areas with low photosynthetic activity.

Three-dimensional distortion, optical errors and alteration of the biocrust images should be taken into account for an image processing approach. In general, consumer-grade NIR-G-B cameras can be used as simple tool for imaging of biological systems. The use of the combination of both imaging techniques allows novel insights into spatial variances of photosynthetic activities in relation to biocrust community and in response to environmental processes. Future combined field observations of NDVI imaging and CFI, and the integration of information about climatic parameters such as rainfall, radiation or temperature can be linked to physiological processes of

biocrusts during the daily and seasonal courses. Additionally, spatial pattern of desiccation and regeneration as well biocrust development can be investigated. Hence, the pattern analysis of biocrusts can provide more precise information of carbon fixation and topsoil carbon cycling, which are important parameters of soil quality and function.

Acknowledgement

The authors thank the Stiftung für Naturlandschaften Brandenburg in Lieberose for providing access to the investigation area. Maik Veste thanks the Geschwister-Staude-Stiftung for financial support through the University of Hohenheim.

References

Bauriegel, E., Giebel, A., Geyer, M., Schmidt, U., Herppich, W.B., 2011a. Early detection of Fusarium infection in wheat using hyper-spectral imaging. Comput. Electron. Agric. 75, 304–312.

Bauriegel, E., Giebel, A., Herppich, W.B., 2011b. Hyperspectral and chlorophyll fluorescence imaging to analyse impacts of *Fusarium culmorum* on photosynthetic integrity of infected wheat ears. Sensors 11, 3765–3779.

Bauriegel, E., Herppich, W.B., 2014. Hyperspectral and chlorophyll fluorescence imaging for early detection of plant diseases, with special reference to *Fusarium spec.* infections on wheat. Agriculture 4, 32–57.

Belnap, J., Lange, O.L. (Eds.), 2003. Biological soil crusts: structure, function and management. Springer, Heidelberg.

Bhardwaj, S., Mittal, A., 2012. A survey on various edge detector techniques. Procedia Technology 4, 220–226.

Bowker, M.A., Maestre, F.T., Escolar, C., 2010. Biological soil crusts as a model system for examining the biodiversity-function in soils. Soil Biol. Biochem. 42, 405–417.

Brankatschk, R., Fischer, T., Veste, M., Zeyer, J., 2013. Succession of N cycling processes in biological soil crusts on a central European inland dune. FEMS Microbiol. Ecol. 83, 149–160.

Breckle, S.-W., Yair, A., Veste M. (Eds.), 2008. Arid Dune Ecosystems – The Nizzana Sands in the Negev Desert, Springer, Heidelberg.

Bresinsky, A., Körner, C., Kadereit, J.W., Neuhaus, G., Sonnewald, U., 2008. Strasburger - Lehrbuch der Botanik, 36. ed., Spektrum Akademischer Verlag, Heidelberg.

Büdel, B., Veste, M., 2008. Biological soil crusts. In: Breckle, S.-W., Yair, A., Veste, M. (Eds.), Arid Dune Ecosystems — The Nizzana Sands in the Negev Desert. Ecologcial Studies, Vol. 200, Springer, Heidelberg, pp. 149–155.

Burgheimer, J., Wilske, B., Maseyk, K., Karnieli, A., Zaady, E., Yakir, D., Kesselmeier, J., 2006. Relationships between Normalized Difference Vegetation Index (NDVI) and carbon fluxes of biologic soil crusts assessed by ground measurements, J. Arid Environ. 64, 651–669.

Couradeau, E., Karaoz, U., Lim, H.C., da Rocha, U.N., Northern, T., Brodie, E., Garcia-Pichel, F., 2016. Bacteria increase arid-land soil surface temperature through the production of sunscreens. Nature Comm. 7, 10373.

Cutler, N.A., Belyea, L.R., Dugmore, A.J., 2008. The spatiotemporal dynamics of a primary succession. J. Ecol. 96, 231–246.

Dümig, A., Veste, M., Hagedorn, F., Fischer, T., Lange, P., Spröte, R., Kögel-Knabner, I., 2014. Water-soluble organic matter from biological soil crusts induces initial formation of sandy temperate soils. Catena 122, 196–208.

DWD (Deutscher Wetterdienst, Bundesministerium für Verkehr und digitale Infrastruktur online) 2014. Mittelwerte 30-jähriger Perioden. Mittelwerte für den aktuellen Stationsstandort (2012) für den Zeitraum 1981-2010, URL: http://www.dwd.de/bvbw/appmanager/bvbw/dwdwww Desktop?_nfpb=true&_pageLabel=dwdwww_menu2_presse&T98029gsbDocumentPath=Navigation%2FPresse%2FKlimainformationen%2Fbeschreibung__mittelwerte__node.html%3F__nnn%3Dtrue, [28.04.2014].

DWD (Deutscher Wetterdienst, Bundesministerium für Verkehr und digitale Infrastruktur online) 2017. Klimadaten Deutschland – Monatswerte Station Cottbus, URL: http://www.dwd.de/DE/leistungen/klimadatendeutschland/klimadatendeutschland.html?nn=16102 , [31.01.2017].

Eckert, R.E., Peterson, F.F., Meurisse, M.S., Stephens, J.L., 1986. Effects of soil-surface morphology on emergence and survival of seedlings in big sagebrush communities. J. Range Manage 39, 414–420.

Elbert, W., Weber, B., Burrows, S., Steinkamp, J., Büdel, B., Andreae, M.O., Pöschl, U., 2012. Contribution of cryptogamic covers to the global cycles of carbon and nitrogen. Nature Geosciences 5, 459–462.

Eldridge, D.J., Greene, R.S.B., 1994. Microbiotic soil crusts: a review of their roles in soil and ecological processes in the rangeland of Australia. Aust. J. Soil Res. 32, 389–415.

Ellenberg, H., Leuschner, C., 2010. Vegetation Mitteleuropas mit den Alpen – in ökologischer, dynamischer und historischer Sicht. Ulmer – UTB, Stuttgart.

Fischer, T., Veste, M., Eisele, A., Bens, O., Spyra, W., Hüttl, R.F., 2012. Small scale spatial heterogeneity of Normalized Difference Vegetation Indices (NDVIs) and hot spots of photosynthesis in biological soil crusts. Flora 207, 159–167.

Garcia-Pichel, F., Belnap, J., 1996. Microenvironments and microscale productivity of cyanobacterial desert crusts. J. Phycol. 32, 774–-782.

Gypser, S., Herppich, W.B., Fischer, T., Lange, P., Veste, M., 2016. Photosynthetic characteristics and their spatial variance of biological soil crust covering initial soils of post-mining sites in Lower Lusatia. Flora 220, 103–116.

Gypser, S., Veste, M., Fischer, T., Lange, P., 2015. Formation of soil lichens crusts at reclaimed post-mining sites, lower Lusatia, north-east Germany. Graphis Scripta 27, 3–14.

Gypser, S., Veste, M., Fischer, T., Lange, P., 2015b. Infiltration and water retention of biological soil crusts on reclaimed soils of former open-cast lignite mining sites in Brandenburg, north-east Germany. J. Hydrol. Hydromech. 64, 1–11.

Herppich, M., Herppich, W.B., von Willert. D.J., 1994. Influence of drought, rain and artificial irrigation on photosynthesis, gas exchange and water relations of the fynbos plant *Protea acaulos* (L.) Reich at the end of the dry season. Bot. Acta 107, 440–450.

Johansen, J.R., 1993. Cryptogamic crusts on semiarid and arid lands of North America. J. Phycol. 29, 140–147.

Karnieli, A., Tsoar, H., 1995. Spectral reflectance of biogenic crust developed on desert dune sand along the Israel-Egypt border. Int. J. Remote Sensing 16, 369–374.

Kidron, G.J., Yaalon, D.H., Vonshak, A., 1999. Two causes for runoff initiation on microbiotic crusts: hydrophobicity and pore clogging. Soil Sci. 164, 18–27.

Läderach, S., Lack, N., Nebiker, S., 2015. Micro-UAV und neue leichtgewichtige Multispektralsensoren für agronomische Anwendungen. Bornimer Agrartechnische Berichte 88, 25–39.

Li, B., Gao, J., Wang, X., Ma, L., Cui, Q., Veste, M., 2016. Effects of biological soil crusts on water infiltration and evaporation Yanchi Ningxia, Maowusu Desert, China. Int. J. Sediment Res. 31, 311–323.

Maestre, F.T., Bowker, M.A., Cantón, Y., Castillo-Monroy, A.P., Cortina, J., Escolar, C., Escudero, A., Lázaro, R., Martínez, I., 2011. Ecology and functional roles of biological soil crusts in semi-arid ecosystems of Spain. J. Arid Environ. 75, 1282–1291.

Maestre, F.T., Bowker, M.A., Eldrige, D.J., Cortina, J., Lázaro, R., Gallardo, A., Delgado-Baquerizo, M., Berdugo, M., Castillo-Monroy, A., Valencia, E., 2016. Biological soil crusts as a model in ecology. In: Weber, B., Büdel, B., Belnap, J. (Eds.), Biological soil crusts: an organizing principle in drylands. Ecological Studies, Vol. 226, Springer, Heidelberg, pp. 407–425.

Porada, P. Weber, B., Elbert, W., Pöschl, U., Kleidon, A., 2014. Estimating impacts of lichens and bryophytes on global biogeochemical cycles. Global Biochem. Cy. 28, 71–85.

Pushkareva, E., Elster, J., 2013. Biodiversity and ecological classification of cryptogamic soil crusts in the vicinity of Petunia Bay, Svalbard. Czech Polar Reports 3, 7–18.

Raanan, H., Felde, V.J.M.N.L., Peth, S., Drahorad, S., ionescu, D., Eshkol, G., Treves, H., Felix-Henningsen, P., Berkowitz, S.M., Keren, N., Horn, R., Hagemann, M., Kaplan, A., 2015. Three-

dimensional structure and cyanobacterial activity within a desert biological soil crust. Environ. Microbiol. 18, 372–383.

Raggio, J., Pintado, A., Vivas, M., Sancho, L.G., Büdel, B., Colesie, C., Weber, B., Schroeter, B., Lázaro, R., Green, T.G.A., 2014. Continuous chlorophyll fluorescence, gas exchange and microclimate monitoring in a natural soil crust habitat in Tabernas badlands, Almería, Spain: progressing towards a model to understand productivity. Biodivers. Conserv. 23, 1809–1826.

Rodriguez-Caballero, E., Knerr, T., Weber, B., 2015. Importance of biocrusts in dryland monitoring using spectral indices. Remote Sens. Environ. 170, 32–89.

Russow, R., Veste, M., Böhme, F., 2005. A natural 15-N approach to determine the biological fixation of atmospheric nitrogen by biological soil crusts of the Negev desert. Rapid Commun. Mass Spectrom. 19, 3451–3456.

Schaaf, W., Bens, B., Fischer, A., Gerke, H.H., Gerwin, W., Grünewald, U., Holländer, H.M., Kögel-Knabner, I., Mutz, M., Schloter, M., Schulin, R., Veste, M., Hüttl, R.F., 2011. Patterns and processes of initial terrestrial-ecosystem development. J. Plant Nutr. Soil Sci. 174, 229–239.

Schroeter, B., Green, T.G.A., Seppelt, R.D., Kappen, L., 1992. Monitoring photosynthetic activity of crustose lichens using a PAM-2000 fluorescence system. Oecologia 92, 457–462.

Schroeter, B., Kappen, L., Moldaenke, C., 1991. Continuous in situ recording of the photosynthetic activity of antarctic lichens established methods and a new approach. Lichenologist 23, 253–265.

Veste, M., Heusinkveld, B.G., Berkowicz, S.M., Breckle, S.-W., Littmann, T., Jacobs, A.F.G. 2008. Dew formation and biological crusts activity. In: Breckle, S.-W., Yair, A., Veste, M.

(Eds.), Arid Dune Ecosystems — The Nizzana Sands in the Negev Desert. Ecologcial Studies, Vol. 200. Springer, Heidelberg. pp. 305–318.

Veste, M., Littmann, T. 2006. Dewfall and its geo-ecological implication for biological surface crusts in desert sand dunes (north-western Negev, Israel). J. Arid Land Stud. 16, 139–147.

Veste, M., Littmann, T., Friedrich, H., Breckle, S.-W., 2001. Microclimatic boundary conditions for activity of soil lichen crusts in sand dunes of the north-western Negev desert, Israel. Flora 196, 465–476.

von Willert, D.J., Matyssek, R., Herppich, W.B., 1995. Experimentelle Pflanzenökologie. Grundlagen und Anwendungen. Georg Thieme Verlag, Stuttgart.

Weber, B., Büdel, B., Belnap, J. (Eds.), 2016. Biological soil crusts: an organizing principle in drylands. Ecological Studies, Vol. 226, Springer, Heidelberg.

Weber, B., Olehowski, C., Knerr, T., Hill, J., Deutschewitz, K., Wessels, D.C.J., Eitel, B., Büdel, B., 2008. A new approach for mapping of biological soil crusts in semidesert areas with hyperspectral imagery. Remote Sens. Environ. 112, 2187–2201.

Xiao, B., Wang, H., Fan, J., Fischer, T., Veste, M., 2013. Biological soil crusts decrease soil temperature in summer and increase soil temperature in winter in semiarid environment. Ecol. Eng. 58, 52–56.

Yair, A., Almog, R., Veste, M., 2011. Differential hydrological response of biological topsoil crusts along a rainfall gradient in a sandy arid area: Northern Negev desert, Israel. Catena 87, 326–333.

Yu, J., Guan, P., Zhang, X., Ma, N., Steinberger, Y., 2016. Biocrusts beneath replanted shrubs account for the enrichment of macro- and micronutrients in semi-arid sandy land. J. Arid Environ. 128, 1–7.

Captions

Fig. 1. Empirical cumulative distribution functions of (A) F_0 and (B) F_m for all biocrust samples, where (I) marks the tonal value range from 0 to 25, (II) marks the tonal value range from 25 to 30 for F_0 and 25 to 60 for F_m (grey highlighted), and (III) marks the tonal value range from 30 to 255 for F_0 and 60 to 255 for F_m.

Fig. 2. RGB, NIR-G-B, and gray-valued NDVI images of the different biocrust types sampled at Lieberose.

Fig. 3. RGB, F_0, F_m, and F_v/F_m images of the biocrust types sampled at Lieberose.

Fig. 4. Matching of NDVI and CFI of BC 1 including (A) Clipped RGB image of biocrust sample BC 1 with marked areas of (B) NDVI (blue), (C) F_0 and F_m (red), (D) the overlapping areas of NDVI and chlorophyll fluorescence and (E) mutual areas of NDVI and chlorophyll fluorescence (green). "Low" describes images with marked areas representing low chlorophyll fluorescence and pixels with tonal values in the range 25 to 35 for F_0 and 25 to 60 for F_m. "High" describes images with marked areas representing high chlorophyll fluorescence and pixels with tonal values in the range 35 to 255 for F_0 and 60 to 255 for F_m.

Fig. 5. Matching of NDVI and CFI of BC 5 including (A) Clipped RGB image of biocrust sample BC 5 with marked areas of (B) NDVI (blue), (C) F_0 and F_m (red), (D) the overlapping areas of NDVI and chlorophyll fluorescence and (E) mutual areas of NDVI and chlorophyll fluorescence (green). "Low" describes images with marked areas representing low chlorophyll fluorescence and pixels with tonal values in the range 25 to 35 for F_0 and 25 to 60 for F_m. "High" describes images with marked areas representing high chlorophyll fluorescence and pixels with tonal values in the range 35 to 255 for F_0 and 60 to 255 for F_m.

Fig. 6. Matching of NDVI and CFI of BC 4 including (A) Clipped RGB image of biocrust sample

BC 4 with marked areas of (B) NDVI (blue), (C) F_0 and F_m (red), (D) the overlapping areas of NDVI and chlorophyll fluorescence and (E) mutual areas of NDVI and chlorophyll fluorescence (green). “Low” describes images with marked areas representing low chlorophyll fluorescence and pixels with tonal values in the range 25 to 35 for F_0 and 25 to 60 for F_m. “High” describes images with marked areas representing high chlorophyll fluorescence and pixels with tonal values in the range 35 to 255 for F_0 and 60 to 255 for F_m.

Appendix

Fig. A1. Matching of NDVI and CFI of BC 2 including (A) Clipped RGB image of biocrust sample BC 2 with marked areas of (B) NDVI (blue), (C) F_0 and F_m (red), (D) the overlapping areas of NDVI and chlorophyll fluorescence and (E) mutual areas of NDVI and chlorophyll fluorescence (green). “Low” describes images with marked areas representing low chlorophyll fluorescence and pixels with tonal values in the range 25 to 35 for F_0 and 25 to 60 for F_m. “High” describes images with marked areas representing high chlorophyll fluorescence and pixels with tonal values in the range 35 to 255 for F_0 and 60 to 255 for F_m.

Fig. A2. Matching of NDVI and CFI of BC 3 including (A) Clipped RGB image of biocrust sample BC 3 with marked areas of (B) NDVI (blue), (C) F_0 and F_m (red), (D) the overlapping areas of NDVI and chlorophyll fluorescence and (E) mutual areas of NDVI and chlorophyll fluorescence (green). “Low” describes images with marked areas representing low chlorophyll fluorescence and pixels with tonal values in the range 25 to 35 for F_0 and 25 to 60 for F_m. “High” describes images with marked areas representing high chlorophyll fluorescence and pixels with tonal values in the range 35 to 255 for F_0 and 60 to 255 for F_m.

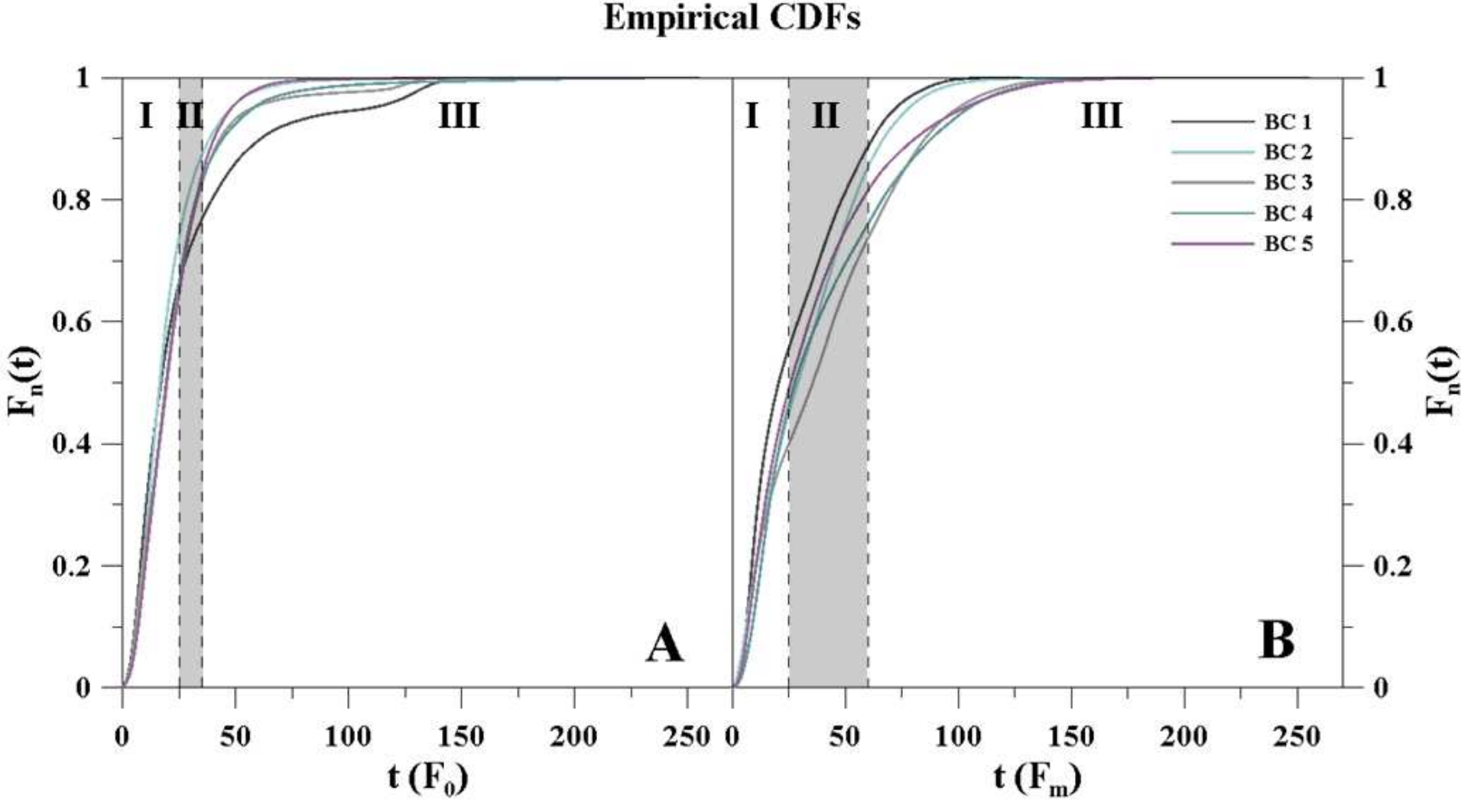
Empirical CDFs
I
II
III
A
B
BC 1
BC 2
BC 3
BC 4
BC 5
$F_n(t)$
$t (F_0)$
$t (F_m)$
0
0.2
0.4
0.6
0.8
1
0
50
100
150
200
250

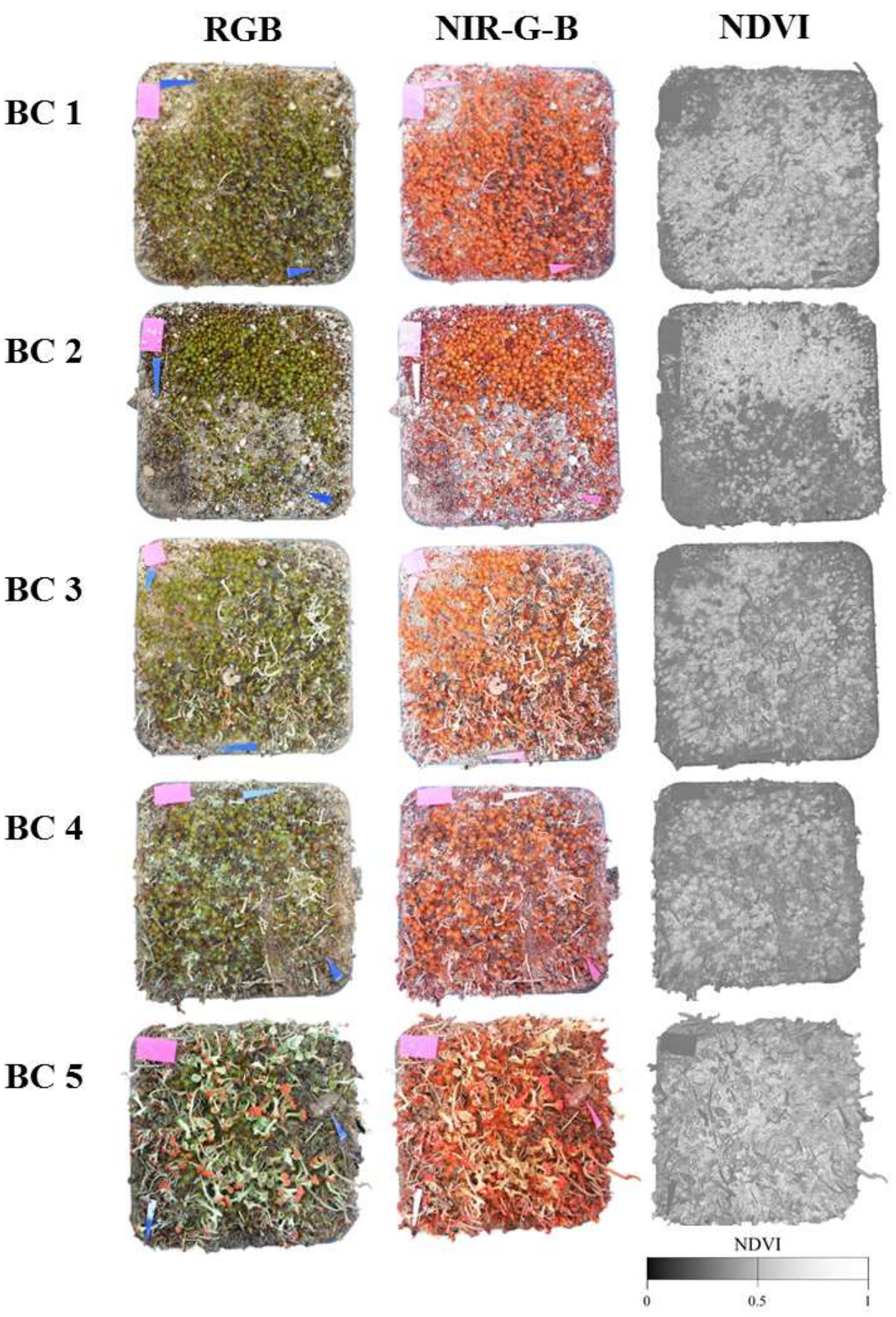
RGB
NIR-G-B
NDVI
BC 1
BC 2
BC 3
BC 4
BC 5
NDVI
0
0.5
1

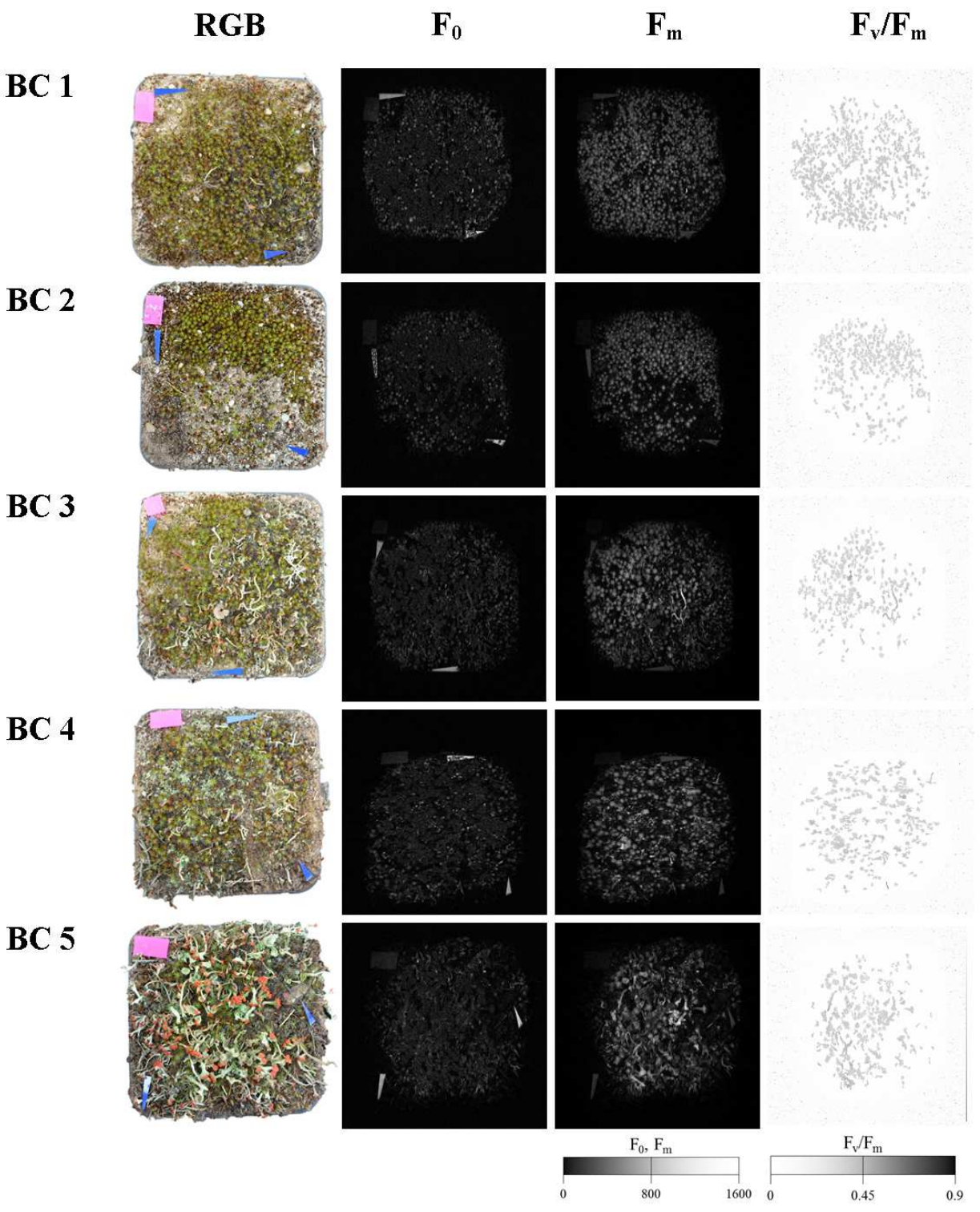
RGB
F_0
F_m
F_v/F_m
BC 1
BC 2
BC 3
BC 4
BC 5
F_0, F_m
0
800
1600
F_v/F_m
0
0.45
0.9

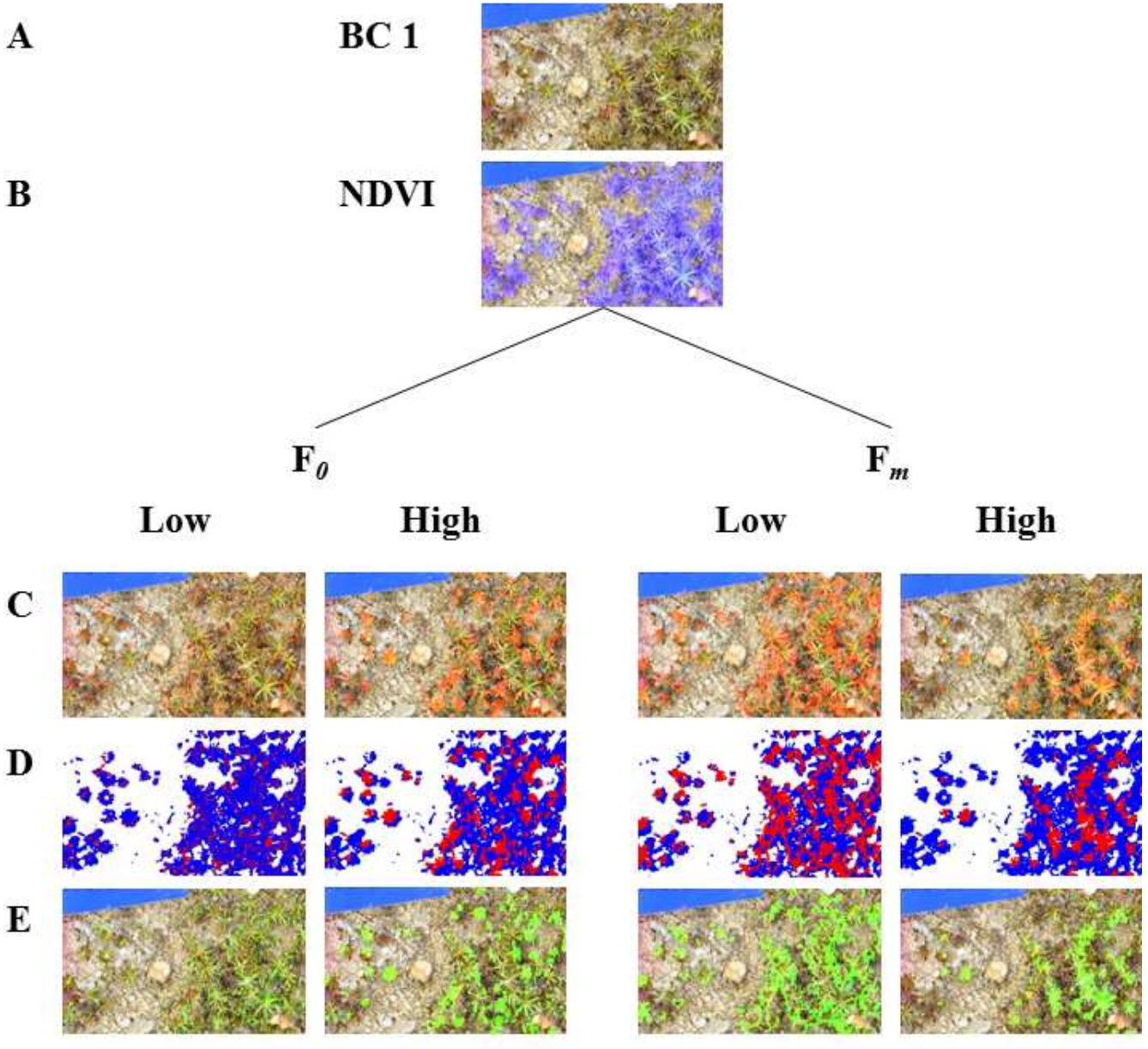
A
BC 1
B
NDVI
F0
Fm
Low
High
Low
High
C
D
E

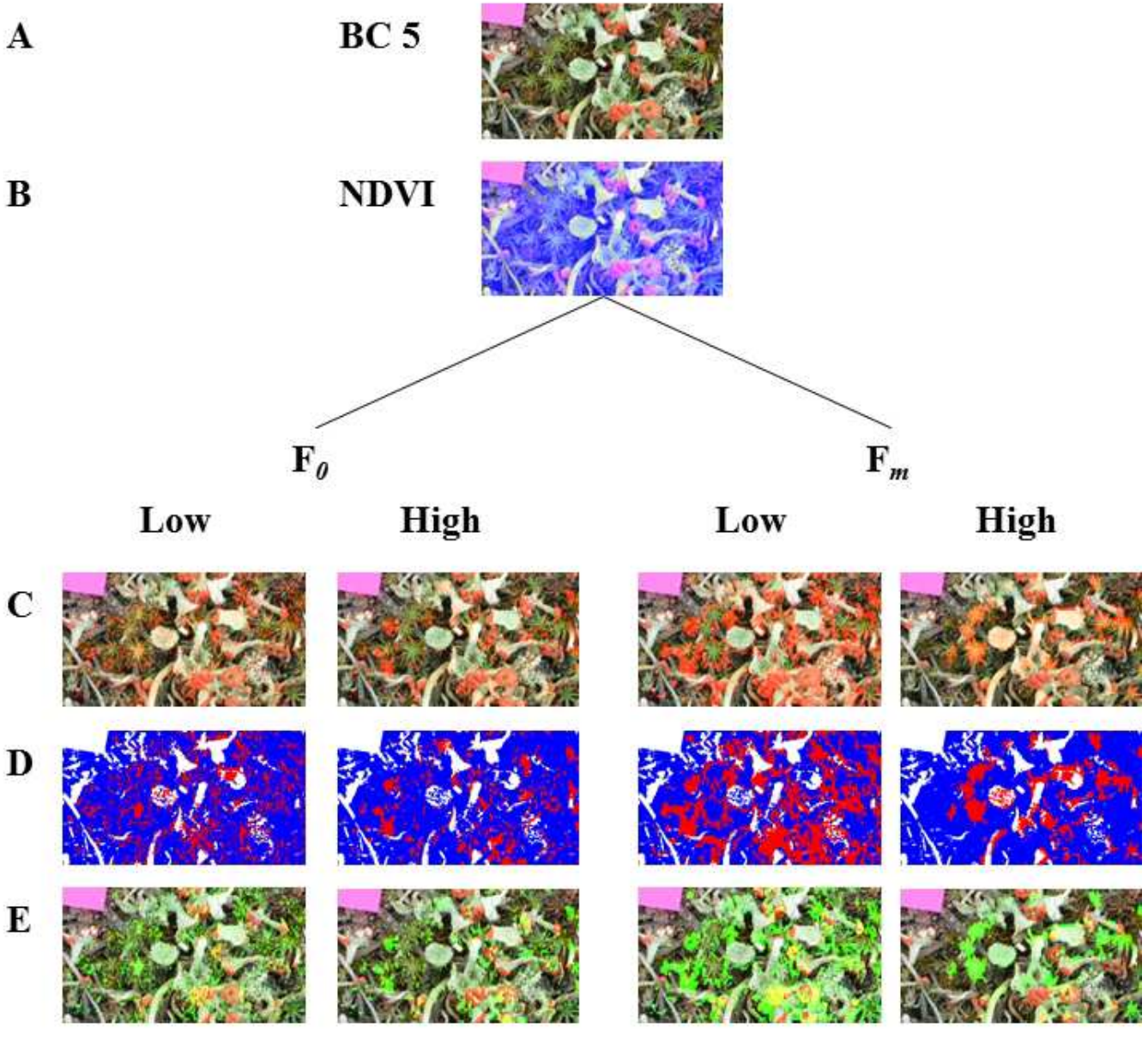
A
BC 5
B
NDVI
F0
Fm
Low
High
Low
High
C
D
E

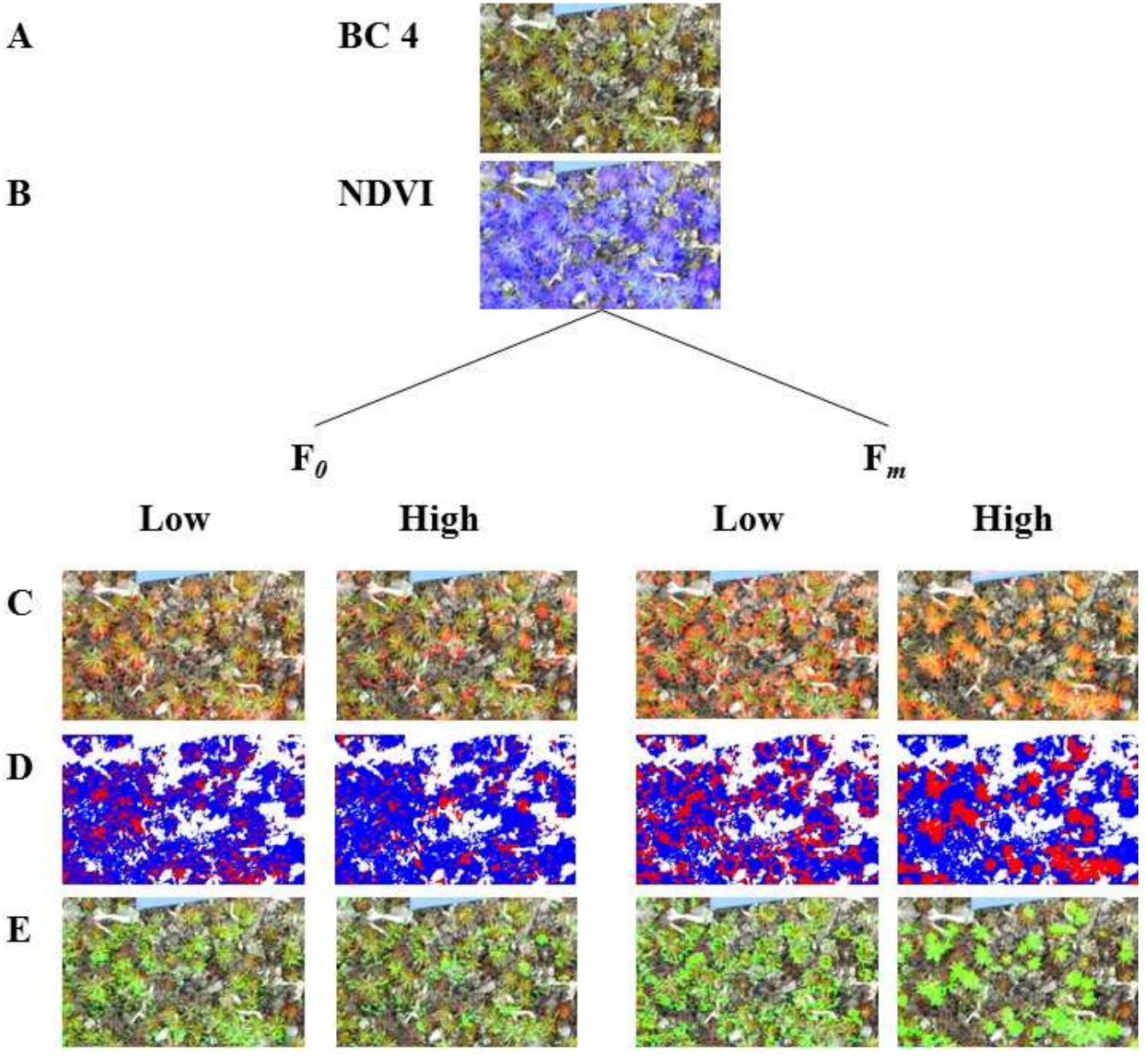
A
BC 4
B
NDVI
F0
Fm
Low
High
Low
High
C
D
E

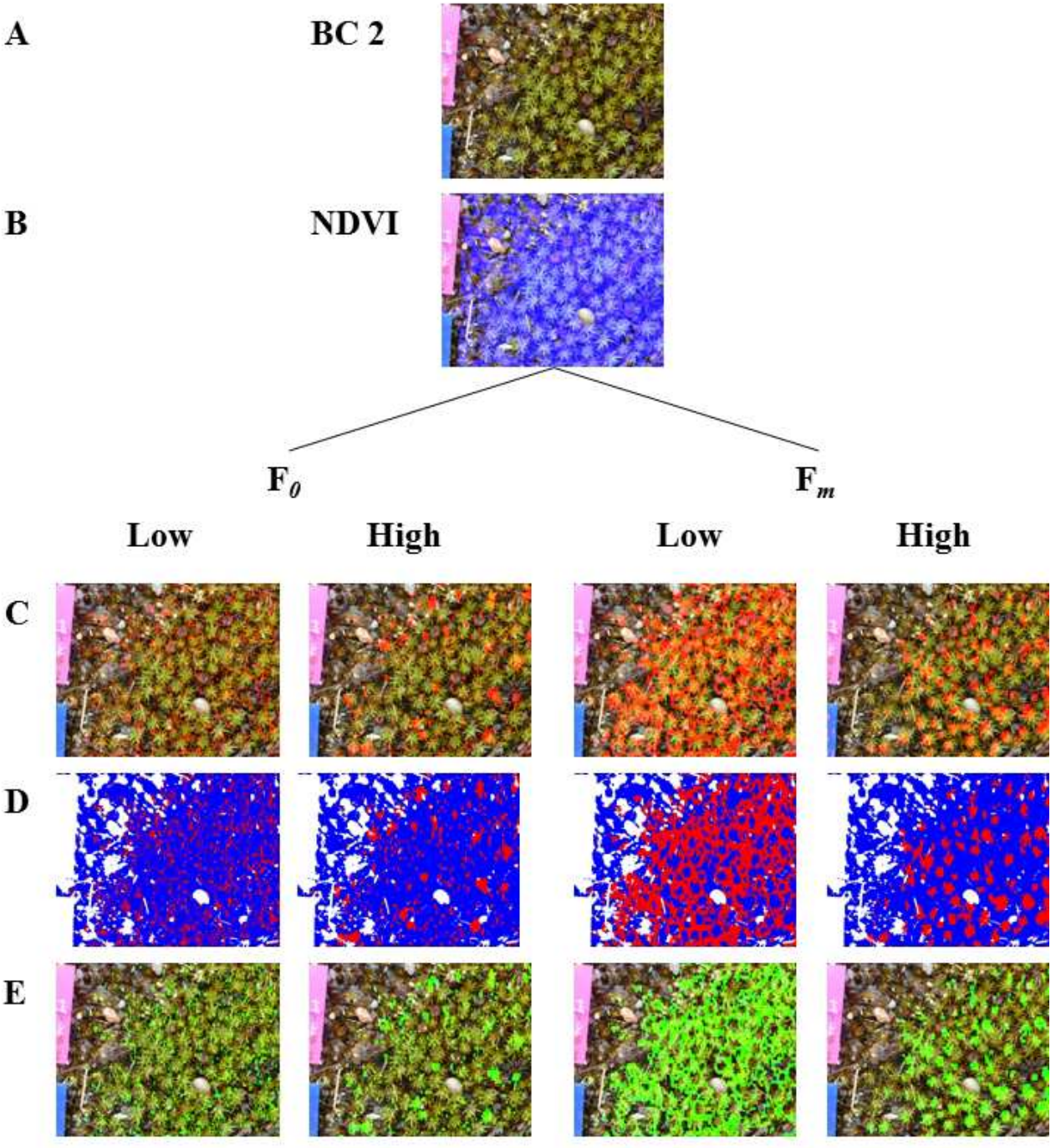
A
BC 2
B
NDVI
F0
Fm
Low
High
Low
High
C
D
E

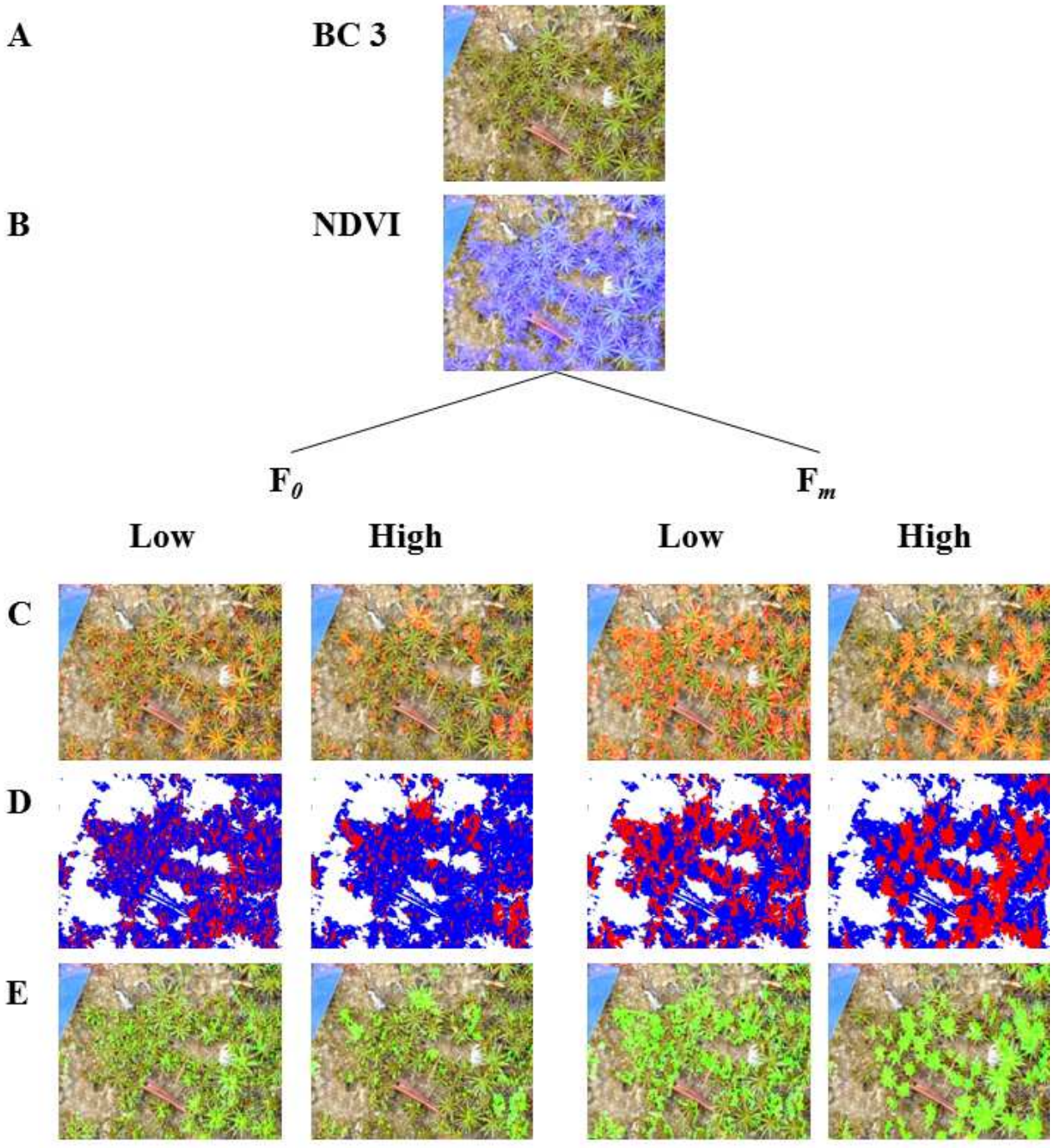
A
BC 3
B
NDVI
F0
Fm
Low
High
Low
High
C
D
E

Tables

Tab. 1. Calculated NDVI, F_0, F_m and F_v/F_m for all biocrust samples.

Biocrust sample	NDVI	F_0	F_m	F_v/F_m
BC 1	0.65	120	438	0.724
BC 2	0.59	106	427	0.751
BC 3	0.60	140	539	0.742
BC 4	0.60	146	552	0.735
BC 5	0.68	147	557	0.736

Tab. 2. Area ratios of NDVI, F_0 and F_m related to the clipped RGB-image and the percentage of matching of NDVI with F_0 and NDVI with F_m.

Biocrust type	**BC 1**	**BC 2**	**BC 3**	**BC 4**	**BC 5**
	Matching Low Chlorophyll fluorescence [%]				
NDVI	47,7	79,7	64,4	68,7	84,0
F_0	8,1	13,0	16,3	14,8	16,4
F_m	21,5	37,6	25,7	22,2	30,2
Match NDVI/F_0	17,01	16,31	25,37	21,47	19,48
Match NDVI/F_m	45,05	47,13	39,86	32,35	35,97
	Matching High Chlorophyll fluorescence [%]				
NDVI	47,7	79,7	64,4	68,7	84,0
F_0	13,6	10,5	11,7	9,9	12,5
F_m	10,2	13,8	24,0	20,0	14,3
Match NDVI/F_0	28,5	13,2	18,1	14,4	14,9
Match NDVI/F_m	21,4	17,3	37,3	29,1	17,0